Design of Nonoverconstrained Energy-Efficient Multi-Axis Servo Presses for Deep-Drawing Applications

Design of Non-overconstrained Energy-efficient Multi-axis Servo Presses for Deep-Drawing Applications*

Francesco Meoni, Marco Carricato
DIN-Department of Industrial Engineering
University of Bologna, Bologna, Italy
francesco.meoni2@unibo.it, marco.carricato@unibo.it

Servo-actuated presses may provide maximum pressing force at any ram position in the same manner that hydraulic presses do, while offering several benefits in terms of precision, energy-conversion efficiency and simplicity, due to their lack of hydraulic circuitry and oil. Several press builders have developed servo-actuated presses; however, issues relating to overconstrained multi-axis architecture have been neglected. The present study proposes an innovative method to avoid overconstrained architectures in multi-axis presses, by implementing a family of modular parallel mechanisms that connect multiple servo-axes to the press ram. Parallel mechanisms, which have application in several fields of robotics and industrial automation, exhibit important benefits for the application at hand, including high load capacity, stiffness and compactness. A biaxial industrial servo press prototype with a non-overconstrained and modular architecture was built and presented as a proof of concept. Each axis comprises a servomotor, a gearbox reducer and a ball-screw transmission. It is shown that such a press may be constructed from commercially available components, achieving high energy efficiency and high press force with relatively simple construction. A direct comparison with an equivalent hydraulic-press model is carried out, thus highlighting the servo press energy efficiency.

1 Introduction

Electronically-controlled servo drives are primarily used in industry as motors for the movement of manufacturing components or the actuation of tools. Recently, several press builders have developed next-generation pressing machines actuated by servo technology. This type of presses maintain the flexibility of hydraulic presses while offering the unique benefits of a mechanical press: high speed and accuracy can be achieved without using hydraulic-oil, while, as with hydraulic technology, maximum pressing force is available at any ram position and large strokes may be performed.These features, along with servo-drive digital control, allow the execution of a wide range of movements with improved accuracy, including those specific to the majority of high-load pressing processes. The absence of hydraulic oil is a benefit from many points of view: it is more eco-sustainable, creates a cleaner working environment and eliminates the requirement for oil distribution circuits, thus avoiding issues related to piping and oil disposal, as well as removing the power consumption of auxiliary devices. Furthermore, there is no energy-conversion loss between mechanical and hydraulic motion, thus yielding higher energy efficiency.

The first applications of servomotors in pressing operations concerned standard mechanical press architecture, where a crank-lever mechanism was actuated by an electric motor along with a clutch and a flywheel. The flywheel allowed storage of kinetic energy while the motor was disengaged, subsequently being released during the pressing phase while relying on a crank-lever mechanism to generate peak force. In order to provide the necessary power, both (fixed-speed) induction motors and servomotors, appropriately coupled, were mounted together on the press, in the so-called *hybrid* architecture [1–7]. The induction motor provided the necessary energy to complete the process while the servomotor was responsible for precise regulation. Though this approach saw integration of servomotors, maximum force was only available at specific positions, i.e. in the proximity of the dead centre of the linkage.

To achieve complete machine flexibility, as with hydraulic presses, maximum force must be available at any position over large strokes. To this end, electric presses equipped solely with servo-actuated axes have been developed. The generic servo-actuated axis (also referred to as *servo axis*) is composed of a servomotor that provides rotating motion, and a constant-speed-ratio mechanical transmission that transforms the latter into linear movement for the press end-effector. Typically, ball or roller screw transmissions are preferred due to their high mechanical efficiency, back-drivability, backlash control, and precision. State-of-the-art servo presses of this type were presented in [8], with servomotors and related technologies analyzed in the context of major applications in sheet and bulk metal forming. However, recirculating-body screws for severe dynamic loads are difficult to manufacture and very expensive. Accordingly, they are often the bottleneck of press design, posing technical and economical limits to the admissible load that a single servo axis may sustain. Hence, to achieve greater press

*A preliminary and partial version of this paper was presented at the 2014 ASME Manufacturing Science and Engineering Conference (MSEC 2014), June 9-13, 2014, Detroit, MI, USA

tonnages, *multi-axis* architecture has been introduced and is now widespread. Hoden Seimitsu Kako (HSK), for example, produce a four-axis ball-screw press [9].

Many issues arise during the design of a multi-axis servo-actuated press if the actuation is redundant, namely if there is a greater number of actuators than degrees of freedom, in a so-called overconstrained architecture. In fact, this kind of layout can achieve motion only when strict geometric conditions are respected, with perfect synchronization between actuators. However, misalignment and control imprecision will always be present in real-world operating conditions. These may cause servomotors to work in conflict with each other, leading to additional internal stresses that affect press structure and motor performance. Furthermore, if ball or roller screw transmissions are used, preload is unpredictably affected and transversal loads may appear, thus hindering transmission operation and drastically reducing their service life. In the worst-case scenario, jamming of linear guides may occur. In seeking to maximize mechanical efficiency and optimize the pressing operation, these problems are non-trivial. To avoid them, the present work proposes a family of non-overconstrained press architectures and presents innovative solutions implementing parallel mechanisms. The latter have been widely used in several fields of robotics and automation, including motion simulators and machine tools [10]. While in a serial mechanism the end-effector is connected to the frame by a single chain of links coupled by motors (cf. typical industrial-robot architectures), in a parallel mechanism the end effector is connected to the base by several chains mounted in parallel, also referred to as *legs*, with motors installed on the frame or close to it. With respect to serial counterparts, parallel machines exhibit higher load capacity and greater stiffness. In this regard, Bai, Guo and Gao [11, 12] proposed parallel mechanisms in order to avoid overconstraint issues caused by actuation redundancy for planar press architectures with 2 or 3 axes and for 6-axis spatial presses. Also, Guo and Gao et al. [13, 14] proposed a servo-mechanical press with redundant actuation driven by two servomotors, using a 2-dof parallel mechanism with mechanical force amplification in order to obtain larger pressing loads.

This paper presents a family of non-overconstrained servo press architectures in which the ram is coupled to n servo axes by means of a parallel mechanism, with $n = 1,...,6$. Suitable arrangements are presented for both planar (with $n = 2,3$) and spatial architectures (with $n = 3,4,5,6$). While the planar and the spatial 6-dof solutions are analogous to those presented in [12], the spatial architectures with $n = 3,4,5$ are presented here for the first time. The presented architectures form a thorough and modular family, with all spatial designs being based on the same two types of legs, i.e. *PUU* and *PUS* (where *P*, *U* and *S* denote prismatic, universal and spherical joints, respectively), thus completing and improving the fundamental results presented in [12]. To achieve full modularity, the paper presents the design of an actuation module, composed of a servomotor, a gear reducer and a ball-screw transmission. This approach achieves press modularity, as the design of each leg and the corresponding servo axis is independent of the total press force and the number of axes used in the press (with the latter being chosen depending on the total press force to be achieved).

In order to show the viability of the proposed approach, the following challenges are addressed:

– the technical feasibility of a heavy-duty servo axis design at an affordable cost, by using state-of-the-art commercial components;
– press energy efficiency, which is supposed to pay off higher press manufacturing costs with respect to hydraulic alternatives.

To this aim, a case study is proposed for a biaxial servo-press: a prototype with a non-overconstrained architecture was built as a proof of concept. A prototype with a 2-dof architecture is considered to be sufficient to address the aforementioned challenges, and was chosen to reduce development costs. The prototype was designed to perform deep-drawing operations characterized by large strokes and time-variable loads, thus accomplishing heavy-duty cycles for industrial production. In order to evaluate energy efficiency, a comparison between such a prototype and an equivalent hydraulic-press model is presented. The hydraulic model is set up by means of commercial components, and the comparison is performed over the same reference cycle (i.e. with the same pressing force, working speed, and cycle time).

2 Non-overconstrained Press Architectures

In order to substitute a hydraulic axis, a servo axis must provide the rated force at any ram position over a relatively large stroke. In this respect, a servo axis with a ball or roller screw transmission may completely substitute a hydraulic axis. The maximum achievable press force, however, is not comparable. A hydraulic axis can easily reach a maximum pressing force of several hundreds tons, whereas for an electric servo axis, as described above, a load capacity in the order of one hundred tons is already a particularly challenging accomplishment. In fact, ball or roller screw transmissions, under the action of significant dynamic loads, are constrained by severe service-life limitations relating to the presence of rotating bodies and to their dynamic behavior (e.g. fatigue, tribological issues etc.). To obtain adequate service life, a specifically designed high-dynamic-load roller or ball screw is necessary. This component is the bottleneck of the axis design, for both its cost and its technical limitations, thus posing an upper limit to the maximum press force that a single servo axis may sustain.

A multi-axis press layout achieves press modularity, while at the same time overcomes single-axis limitations in terms of rated press force. A *module* is represented by a single servo axis, capable of providing a rated press force $\mathbf{Q}_i$. Target total rated press force, $\mathbf{Q}_n$, can be achieved by composing several axes in parallel. This way, if friction is disregarded and all axes are parallel to the ram sliding direction $\mathbf{u}$:

$$\mathbf{Q}_n = Q_n\mathbf{u} = \sum_{i=1}^{n} \mathbf{Q}_i = \left(\sum_{i=1}^{n} Q_i \right) \mathbf{u} \tag{1}$$

Each axis, when considered independently, forms a translational one degree-of-freedom (dof) actuator. When connecting several axes *directly* to the ram, the latter may move if, and only if, all axes share the same translational direction. Thus, all servo axes must be rigorously parallel

and all end-effectors must move in a precisely synchronized manner. These requirements are necessary due to the fact that the described configuration is overconstrained, that is, there is a greater number of actuators (n) than degrees of freedom (one). This particular layout can achieve motion only when strict geometric conditions are respected, which may not be the case under real-world operating conditions. A lack of alignment, even if minimal, is always present, due to clearances, imprecisions during the assembly process or tolerances. Furthermore, since electronic control is responsible for coordination of motor motion during the working phase, small synchronization errors are generated due to the operational tolerance permitted by the control system. These situations can cause servomotors to work in conflict with each other, thus leading to additional internal stresses affecting the press structure, the recirculating-body screw service life, and motor performance. A direct consequence might be that the press does not provide the desired force at the work piece and is therefore unable to complete the designated task. In the worst-case scenario, press failure may occur.

To avoid the foregoing issues, a system has been developed that joins n servo axes to a single ram while avoiding the use of an overconstrained structure. In particular, an n-dof parallel mechanism is used to transmit press forces from the actuators to the ram. This *multiple input-single output* mechanism results in the slide (*output*) motion being the composition of the movements of the n actuators (*inputs*), with actuators being free to move independently with respect to each other.

In the following sections, several mechanisms for a variable number of axes are presented. Planar mechanisms are presented for $n = 2,3$, whereas spatial mechanisms are proposed for $n = 3,4,5,6$.

2.1 Planar mechanisms

A 2-dof planar mechanism for a 2-axis non-overconstrained press is presented in Fig. 1(a). The layout is composed of two parallel servo axes, each providing a press force Q_i, connected to a central guided ram. Two prismatic joints represent servo axes a_1 and a_2. Two rods connect revolute joints centered in A_1 and A_2 to a double hinge centered in B. From this, a third central rod connects to the ram at the revolute joint in C. The ram is free to translate along axis c. In the plane, the mechanism is statically determinate (as can be immediately inferred by applying Grübler formula). In the case of a misalignment h between A_1 and A_2, the central rod rotates by α and point B rotates about point C. This rotation of the central rod "absorbs" the misalignment, thus avoiding bending moments in the structure and conflicts between motors. With an appropriate electronic control, h and therefore α attain very low values. The internal movement of the mechanism is therefore negligible, while the system takes advantage of the benefits of a non-overconstrained geometry.

A planar mechanism for $n = 3$ may be obtained by placing a central platform that connects the 3 actuators to the ram (Fig. 1(b)). Each prismatic joint is connected to the platform by a double-ended revolute joint bar. The result is a three input (axes a_1, a_2 and a_3), single output (axis b) mechanism. In the case of actuator misalignment, the platform is free to translate and rotate in the working plane.

For $n > 3$, the mechanisms connecting the actuators to the ram must be necessarily spatial.

2.2 Spatial Mechanisms

A central platform is used to collect the motion of n inputs via n serial chains, called *legs*. The platform is then connected by a lower leg to the ram, so as to transmit translational motion. In order to improve modularity, only two kinds of legs are used in the following designs. One type, called PUU, comprises a prismatic joint, P, and two universal joints, U, each one composed of two intersecting revolute joints, R. The second kind, called PUS, differs from the former by the substitution of one universal joint, U, with a spherical one, S, obtained by the composition of three concurrent revolute pairs.

The unit twist associated with a prismatic joint is $\boldsymbol{\xi} = [\mathbf{0}^T, \mathbf{s}^T]^T$, with $\mathbf{s}$ being a unit vector along the joint direction; the unit twist associated with a revolute joint is $\boldsymbol{\xi} = [\mathbf{s}^T, (\mathbf{r}\times\mathbf{s})^T]^T$, with $\mathbf{s}$ being a unit vector along the joint axis and $\mathbf{r}$ being any vector from an arbitrarily-chosen reference point to the joint axis. If $\boldsymbol{\xi}^i_j$, $j = 1,\ldots,f^i$, is the unit twist associated with the jth pair of the ith leg (f^i is the total number of 1-dof joints in the leg), the leg constraint space W^i is the null space of the matrix

$$\left(\mathbf{J}^i\right)^T \boldsymbol{\Delta} = \begin{bmatrix} (\boldsymbol{\xi}^i_1)^T \\ \vdots \\ (\boldsymbol{\xi}^i_{f^i})^T \end{bmatrix} \begin{bmatrix} \mathbf{0}_3 & \mathbf{I}_3 \\ \mathbf{I}_3 & \mathbf{0}_3 \end{bmatrix} \tag{2}$$

where $\mathbf{J}^i$ is the leg Jacobian matrix, and $\boldsymbol{\Delta}$ is the operator implementing the reciprocal product between twists and wrenches.

In the case of a (nonsingular) PUU leg (Fig. 2a), $f^i = 5$, $\mathbf{J}^i$ is a 6×5 matrix, and W^i is 1-dimensional. Physically, W^i is spanned by the single wrench that is reciprocal to all joint twists. For example, if the leg universal-joint planes are mutually parallel, the reciprocal wrench is a pure moment $\boldsymbol{\zeta} = [\mathbf{0}^T, \mathbf{n}^T]^T$, with $\mathbf{n}$ being a unit vector perpendicular to the universal-joint planes [15]. In the case of a (nonsingular) PUS leg (Fig. 2b), $f^i = 6$ and $\mathbf{J}^i$ is a 6×6 matrix, so that W^i is 0-dimensional,

When the platform is connected to the frame by $n+1$ legs, with n of them connecting the platform to n servo axes and one connecting the platform to the ram, the overall constraint space, W, acting on the end-effector is the span of the constraint spaces produced by all legs, namely $W = \sum_{i=1}^{n+1} W^i$.

Since the platform motion is given by the twist space reciprocal to W, the platform has $6 - \dim(W)$ freedoms [16, 17]. For the mechanism to have n dof, one must have

$$n = 6 - \dim(W) = 6 - \dim\left(\sum_{i=1}^{n+1} W^i\right) \tag{3}$$

and thus, since the constraint space provided by a PUS leg is

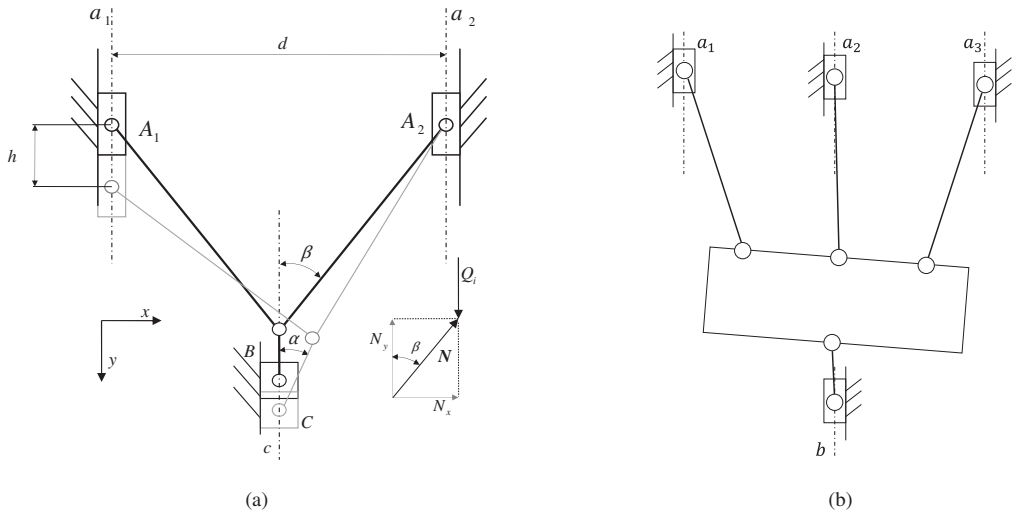

(a) (b)

Fig. 1. Planar non-overconstrained press architectures with (a) 2 dofs, and (b) 3 dofs.

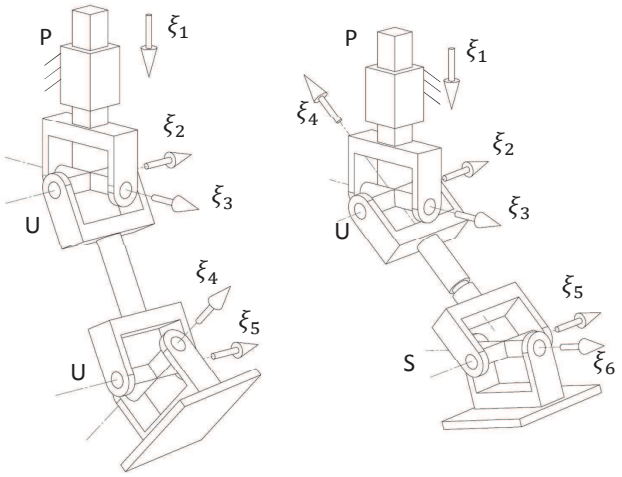

Fig. 2. Joint twists of a PUU (a) and a PUS (b) leg.

0-dimensional,

$$\dim\left(\sum_{i\in\mathcal{N}_{PUU}} W^i\right) = 6-n \tag{4}$$

where $\mathcal{N}_{PUU}$ is the set of indices denoting *PUU* legs. As long as the latter are mounted in such a way that the corresponding reciprocal wrenches are linearly independent [18], $\dim(\sum_{i\in\mathcal{N}_{PUU}} W^i)$ is equal to the number of adopted *PUU* legs. It emerges from the above reasoning that, in order to obtain a press with n equal to 3, 4, 5 or 6, the number of *PUU* legs to be used must be equal to 3, 2, 1 and 0, respectively. Figures 3(a), 3(b), 3(c) and 3(d) show non-overconstrained press architectures with 3, 4, 5 or 6 dof, respectively. In all cases, the prismatic joints in the n upper legs are actuated by servo axes, whereas the lower *PUS* leg connects the platform to the ram. In particular, the upper part of the mechanism in the 3-dof architecture (Fig. 3(a)), with all *PUU* legs mounted in such a way that they exert pure constraint moments, is equivalent to a translational manipulator [19], whereas the upper part of the mechanism in the 6-dof architecture is a variant of the Gough-Stewart manipulator [10].

During operation, all servo axes are controlled with the same motion law. Accordingly, the internal movement of the parallel mechanism in only due to synchronization errors between motors, thus being negligible. In practice, the parallel mechanism operates in a very small neighborhood of its assembly configuration. This fact has important consequences for the simplification of design. In fact, link interference is not an issue in the case at hand, so that joints (in particular universal pairs) may be designed with very limited motion ranges, and the mechanism may be manufactured as a quasi-structure. This guarantees sturdiness and compactness, thus easing structural optimization for heavy-duty applications. Furthermore, Eq. (4) may be verified only in the assembly configuration.

3 Design of a Prototype Biaxial Servo Press

A prototype biaxial servo press with a non-overconstrained architecture was built as a proof of concept (Figures 4-5). A two-axis layout has been chosen so as to highlight the principle issues associated with multi-axis architecture, i.e. the technical feasibility of a heavy-duty servo axis composed of state-of-the-art components at an affordable cost as well as press energy efficiency, while minimizing the prototype realization cost.

3.1 Prototype Specifications

The standard servo press production cycle has been determined while taking into consideration constraints provided by the industrial partners of the *DEFCOM* (Competitiveness in Deformation) project [20]. The prototype is capable of generating a maximum press force of 1200 kN, with each axis providing 600 kN each. The pressing stroke

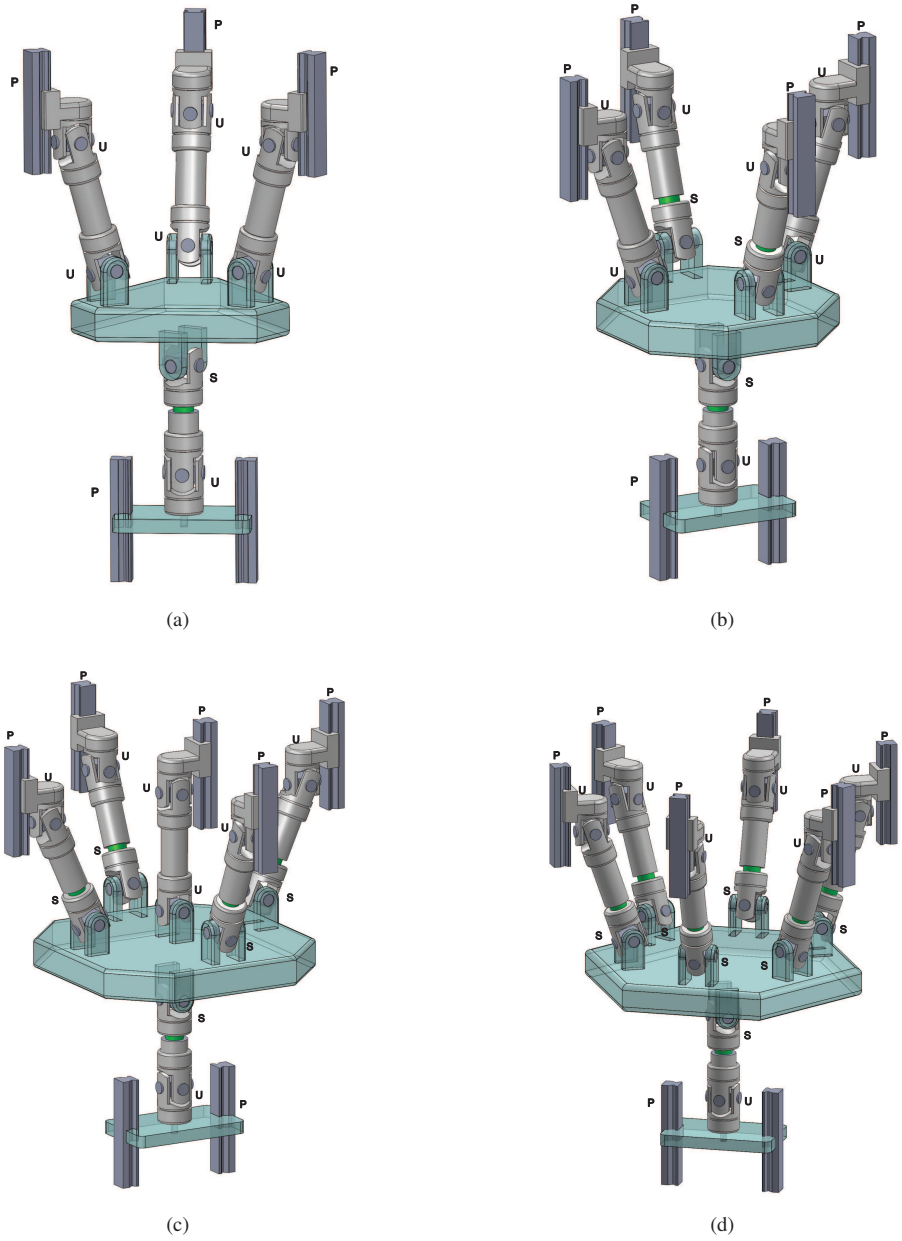

Fig. 3. Spatial non-overconstrained press architectures with (a) 3 dofs, (b) 4 dofs, (c) 5 dofs, and (d) 6 dofs.

is 300 mm, while the maximum stroke, including positioning, is 600 mm. The maximum ram working speed is $\dot{q}_{work} = 50$ mm/s. The rated process power, P, is therefore $P_w = 1200$ kN·50 mm/s= 60 kW. The prototype is designed to undertake heavy-duty manufacturing processes, with a useful service life of roughly 5 million press cycles, with a productivity of 5 cycles per minute. A standard ram motion cycle has been defined that respect the aforementioned constraints. To avoid discontinuity of acceleration, fifth-degree polynomials have been used to generate a piecewise motion function. The ram motion is shown in Fig. 6. In the first part, the ram is positioned at high speed. The velocity is then reduced to 50 mm/s to start the manufacturing process. During the entire deep-drawing operation, from $t = 2.5$ s to $t = 9$ s, the velocity is kept constant. The ram then returns to the initial position. The pressing phase can last up to about half of the entire cycle time, providing a maximum and constant press force throughout the entire process.

The prototype features a *die cushion*, placed at the bottom of the press, which provides a counteracting force up to 600 kN, that is, half the nominal press force. Its motion is equal to that of the ram during pressing, with a stroke of 300 mm. The same servo axis design (i.e. mechanical components, layout etc.) can therefore be used for both the top axes and the die cushion.

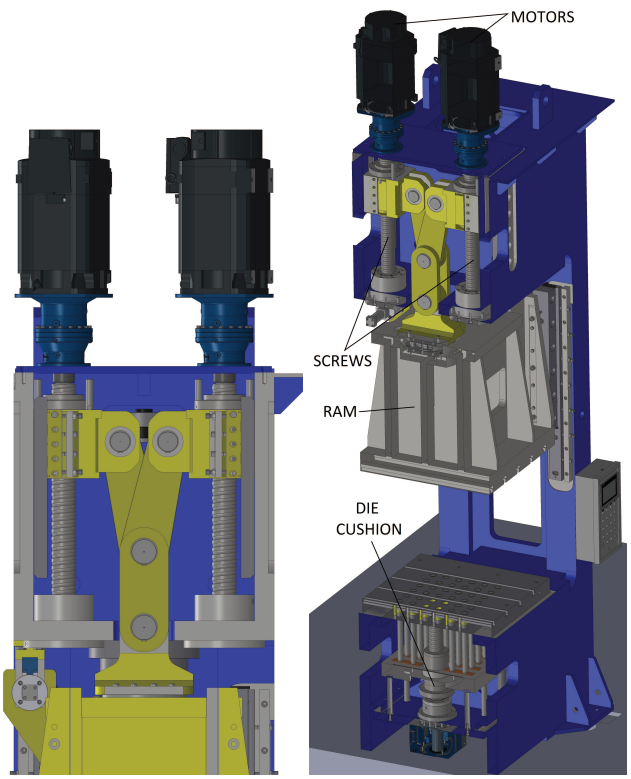

(a) (b)

Fig. 4. Biaxial servo press prototype: (a) CAD section front view, and (b) CAD overall layout.

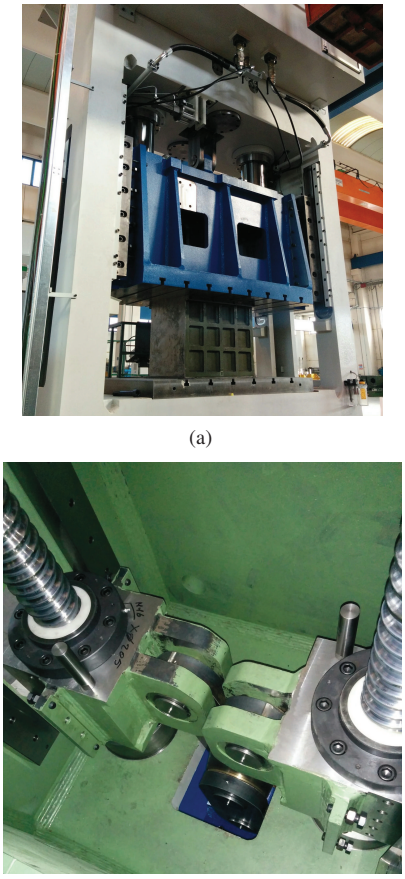

(a) (b)

Fig. 5. Biaxial servo press prototype: (a) global view, and (b) 2-dof actuation mechanism (top view, cover removed).

3.2 Dynamic Model

A lumped-parameter dynamic model of the servo axis has been developed to describe the system behavior and allow appropriate selection of the principle mechanical components. Each servo axis is composed of a servomotor, a reduction gearbox and a ball-screw transmission. The axis motion (i.e. displacement q, velocity $\dot{q}$, and acceleration $\ddot{q}$) is known, as in all cases it may be assumed to be equal to that of the ram. The kinematic chain is modelled using two different types of element:

1) *inertia elements*, which represent the dynamic behavior of components by taking into account inertia effects without considering energy loss.

2) *transmission elements*, which account for variations in velocity and torque (or force), as well as mechanical efficiency across transmission.

Accordingly, each mechanical component is represented by two subsequent blocks: one representing inertial properties and the other accounting for the transmission ratio and mechanical efficiency. The dynamic model of the axis is shown in Fig. 7, where: ω_m and ω_s are the angular velocities of the motor and the screw, respectively; τ_r and τ_s are the transmission ratios of the gear reducer and the ball-screw

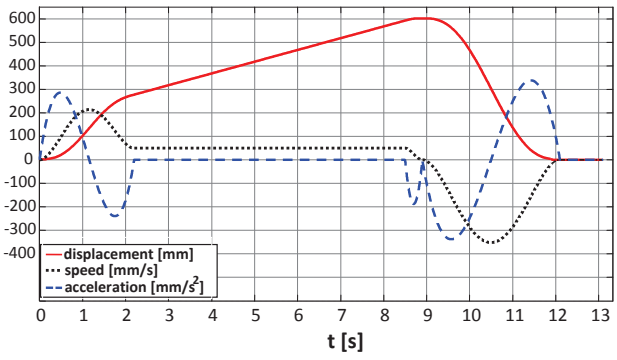

Fig. 6. Reference press cycle of the prototype.

($\tau_s = p_h/2\pi$, with p_h being the screw pitch); C_m is the motor torque; C_{rid1} and C_{rid2} are the input and output torques of the gearbox; F_s is the force on the screw nut; J_{mr} is the combined inertia of motor and gearbox; J_s is the inertia moment of the screw; and m is half the overall ram mass, i.e. $m = 2500$ kg. Energy losses in the gearbox and the screw transmission are

In Sec.2.1 it has been observed that, due to synchronization provided by the servomotor control, misalignments h and α in Fig. 1(a) attain very low values. The effects of these parameters may therefore be disregarded in the dynamic study.

For the sake of simplicity, the mass of the 2-dof mechanism links has been neglected.

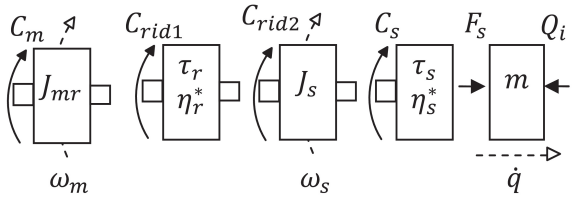

Fig. 7. Lumped parameter model of each servo axis

modeled by stepwise functions that vary according to the direction of power flow, namely

$$\eta_r^* = \begin{cases} \eta_r, & C_{rid1} \geq 0 \\ \frac{1}{\bar{\eta}_r}, & C_{rid1} < 0 \end{cases}; \quad \eta_s^* = \begin{cases} \eta_s, & C_s \geq 0 \\ \frac{1}{\bar{\eta}_s}, & C_s < 0 \end{cases} \tag{5}$$

where η_r and η_s are, respectively, the mechanical efficiencies of the gearbox and the screw when power flows from the motor to the load, and $\bar{\eta}_r$ and $\bar{\eta}_s$ are the mechanical efficiencies of the same components when power flows from the load to the motor.

The motion equation of the servo axis is

$$C_m = \frac{\tau_r \tau_s}{\eta_r^* \eta_s^*} Q_i + \left(J_{mr} + J_s \frac{{\tau_r}^2}{\eta_r^*} + m \frac{{\tau_r}^2 {\tau_s}^2}{\eta_r^* \eta_s^*} \right) \dot{\omega}_m \tag{6}$$

3.3 Component Selection

Commercial components have been selected to provide a press force $Q_i = 600$ kN for each axis. The dynamic model has been used to simulate the behavior of the servo axis and to determine the forces and torques acting on each mechanical component. In the following sections, the main issues encountered during the component selection phase are briefly presented. The list of prototype components is given in Tab. 1, along with the lumped parameters that were used.

3.3.1 Ball-Screw Transmission

Ball-screw systems are typically used when there is the need to have high mechanical efficiency and high precision. In press applications, other than these requirements, they must exhibit durability over time under heavy-duty pressing loads. Few manufacturers can provide high load capacity recirculating-body screws. Due to the relatively small contact surface of a recirculating body, ball screws present several issues relating to their dynamic behavior, such as surface pressure and consequent fatigue failures. Planetary and recirculating roller screws can offer a wider contact surface and present dynamic-load capacities that are generally higher, though they are less efficient and much more expensive. Recirculating-ball screws used in aeronautics industry have a dynamic bearable load comparable to roller screws. Thus, ball-screw transmissions drawn from this sector have been selected due to their higher efficiency and lower cost.

For this application, dynamic load capacity must be taken into account, as press service life is a crucial parameter for an industrial-purpose prototype. Each ball screw is characterized by a basic *dynamic load rating*, C_a, which is used to calculate the fatigue life of screws. It is defined as a constant axial load under which the nominal life reaches one million revolutions. In order to evaluate screw life, the equivalent cycle dynamic load, F_{sm}, is calculated as $F_{sm} = \sqrt[3]{\left(\int_T |F_s|^3 \dot{q} dt\right) / \int_T \dot{q} dt}$, where F_s is the force acting at a given instant on the translating nut and T is the total cycle time. To evaluate $F_s(t)$, and consequently F_{sm}, screw parameters (i.e. pitch, inertia etc.) and servomotor inertia have to be known, so as to simulate the behavior of the entire transmission. Since these parameters are not given before selection, a preliminary screw selection can be based on the maximum torque in the process phase, where speed is constant and inertial effects are ignored. A dynamic simulation can then be performed with the preliminary screw model, thus allowing selection of a new model. The process can be iterated as necessary. Screw service life, S, expressed in millions of revolutions, is defined as $S = (C_a/F_{sm})^3$, thus allowing evaluation of the required dynamic load to achieve a press life of roughly 5 million cycles, corresponding to $S = 150$. A possible choice is the *VRS160* screw [23], with screw diameter $d = 160$ mm, pitch $p_h = 40$ mm and maximum dynamic load $C_a = 1866$ kN. The subsequent useful service life is calculated around 4.4 million cycles, which is deemed to be acceptable.

3.3.2 Servo Motor and Gearbox

To actuate the servo axis, an inverter-controlled asynchronous motor has been selected. An alternative possibility would have been synchronous brushless motor; however, the standard rated power of brushless motors is low compared to the requirements of pressing applications. An inverter-controlled asynchronous motor can provide large power at low cost, while still being able to achieve a suitable dynamic performance for deep drawing applications.

When selecting and sizing the servomotor, several considerations regarding reducer transmission ratio, τ_r, must be made. In principle, it could be possible to directly join the motor to the transmission chain by implementing more expensive, high-torque direct-drive motors. However, when using an asynchronous motor, a gearbox reducer must be employed, so as to match the optimum motor output speed with the screw speed, ω_s. To obtain a value for the motor inertia, a first attempt of motor selection may be undertaken based on the rated process power, P_w. As for the ball screw, this process may be iterated while updating the component layout. Figure 8 shows the mechanical power P provided by a single servo axis, as well as the impact of the transmission ratio. Negative power values indicate that the system is returning energy. This simulation refers to the component selection shown in Tab. 1. Three different phases may be observed. In the first phase, the slider is brought to working position, being firstly accelerated then decelerated by the actuator. In the central phase, the working speed and pressing force are both constant, as is the power consumption. In the third phase, the slide is returned to the initial position, with corresponding acceleration and subsequent deceleration. It is impor-

It will be shown in Sec. 3.3.2 that power flow is from the motor to the load during the working phase, and from the load to the motor during the braking phase of the positioning cycle.

Table 1. Servo axis components of the prototype press

Component	Model	Manufacturer	Lumped Parameters
Motor	$IPH8226-1DB45$	Siemens [21]	$J_{mr} = 1.9538$ kg m^2
Gearbox Reducer	$CI160-3.15$	Rossi [22]	$\tau_r = 0.3175$; $\eta_r = 0.98$; $\bar{\eta}_r = 0.98$
Ball Screw	$VRS160$	Umbra [23]	$J_s = 0.745$ kg m^2; $p_h = 40$ mm; $\tau_s = 0.0064$ mm; $\eta_s = 0.85$; $\bar{\eta}_s = 0.80$

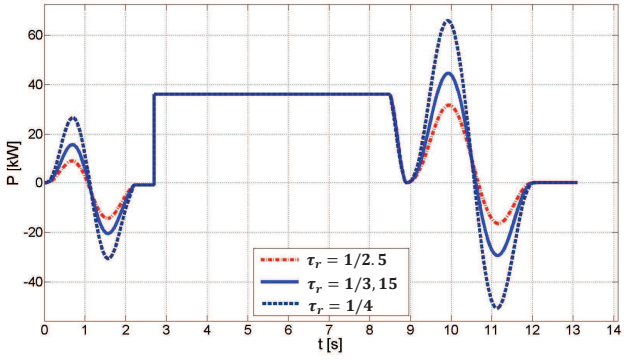

Fig. 8. Mechanical power provided by each axis of the press prototype during the reference cycle, for different values of the gearbox transmission ratio.

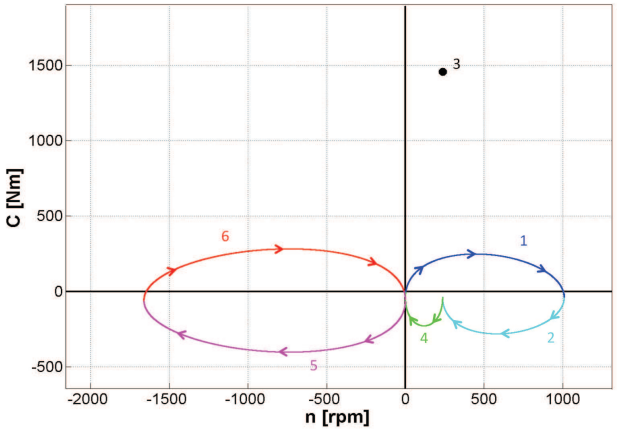

Fig. 9. Motor torque against motor speed during the press cycle: 1) acceleration during downward positioning, 2) deceleration during downward positioning, 3) pressing operation, 4) ram breaking 5) acceleration during upward positioning, 6) deceleration during upward positioning

tant to note the effect of the reducer transmission ratio on the power consumption during the positioning phases. A higher value of τ_r leads to lower peak power during the movement phases. On the other hand, a lower value of τ_r leads to a lower motor torque due to a higher motor speed, ω_m. This particular situation favors asynchronous motor applications, as they are characterized by relatively high nominal speeds. A good, balanced choice of τ_r should be a reasonably low value to minimize motor torque, yet high enough to maintain the absorbed peak power below, or similar to, the rated pressing power.

For example, with a single-stage reduction gearbox with $\tau_r = 3.15$, i.e. $CI160-3.15$ [22], a possible motor selection could be *1PH8226-1DB45* [21]. Figure 9 shows the applied motor torque against motor speed for a single servo axis during the six phases of a press cycle, which are 1) acceleration during downward positioning, 2) deceleration during downward positioning, 3) pressing operation, 4) ram breaking 5) acceleration during upward positioning, 6) deceleration during upward positioning. It should be noted that the servo-actuator operates in all four quadrants and therefore acts both as a motor and a generator.

4 Energy Saving

4.1 Servo Press Energy Recovery

An important feature of servo technology is the possibility to recover kinetic energy during the press cycle, other than avoiding energy conversion losses and dissipation that are characteristic of hydraulic technology. In Fig. 10, the total mechanical power exchanged throughout the *entire* press system is shown. Two contributions are highlighted: the top part and the die cushion. The former refers to the operating servo axes, the latter to the regenerative die cushion placed at the bottom. During the work phase, the energy recovered by the servo axis of the die cushion is instantly used to decrease the energy consumption. While in hydraulic applications the energy used for the counteracting force is ordinarily dissipated, in servo technology this energy can be recovered, as the servo axes can function as a generator. As shown in Fig.8, there are two different phases where the total power assumes negative values and energy is returned by the press system, both during ram deceleration. The energy generated under these conditions can be stored (e.g. in batteries, capacitors etc.) and reused where lower peak powers are required. Alternatively, it can be directly returned to the electricity network.

4.2 Comparison with Hydraulic Technology

Since the prototype is designed to work in industrial environment, it is useful to evaluate the actual impact of the introduction of servo technology in pressing application. In order to evaluate the energy saving ratio, a model of an equivalent hydraulic press has been created. The hydraulic model has been designed to achieve the same performances of the presented servo press prototype, in terms of forces and velocities. A standard motion cycle has been defined (i.e. the ram

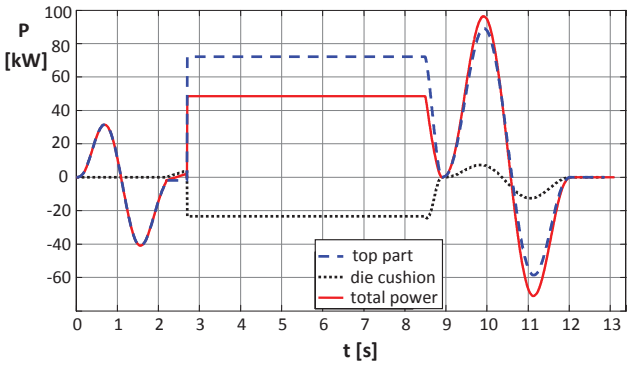

Fig. 10. Total mechanical power exchanged by the press prototype during the reference cycle

Table 2. List of components of the hydraulic circuit of an industrial hydraulic press equivalent to the servo actuated prototype

No.	Component	Model	Man.
1,2	Pump	PV180	Parker
3,7, 11	Two-way Cartridge Seat Valve	LC25	Rexroth
4	Directional Valve	4WEH25E	Rexroth
8	Proportional Throttle Valve	FESXE40	Rexroth
9	Check Valve	M-SR30	Rexroth
10	Directional Valve	4WEH25M	Rexroth
13	Pre-fill Valve	ZSF100	Rexroth

displacement, h, velocity, $\dot{h}$, and acceleration, $\ddot{h}$), in the same way it has been done for the servo axis dynamic model. The two cycles are identical during working phase, while during motion phases a piecewise constant acceleration law of motion has been used for the hydraulic press; the displacement over time is equivalent.

4.2.1 Hydraulic components and circuit

Pressing cylinders have been chosen with bore diameter $D_1 = 180$ mm and rod diameter $D_2 = 125$ mm. In order to have a realistic picture of an industrial hydraulic circuit, commercial components have been selected, with all data regarding pressure drops, flows and dynamic behavior being taken from catalogs and technical manuals. A full list of components is given in Tab. 2

Two cylinders are responsible for providing the pressing force of 1200 kN, while a third cylinder acts as a die cushion. The circuit, shown in Fig. 11, is composed of two axial-piston variable-displacement pumps **1** and **2** feeding two lines: *line R* is connected to the two main cylinders, **5** and **6**, and the oil flux is directed by directional valve **4**; *line L* is dedicated to die cushion **12**, controlled by directional valve **10**. Valves **3**, **7** and **11** are two-way cartridge

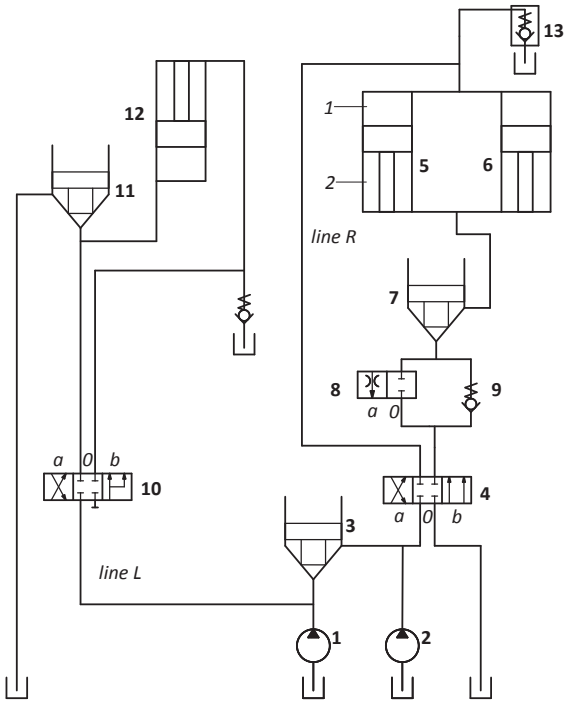

Fig. 11. Hydraulic circuit

valves, and by controlling the power part with appropriate pilot control valves, they can perform pressure control, directional and throttling functions or a combination of these. Proportional cartridge throttle valve **8** controls the oil flow rate.

During pressing phase, the two-way cartridge valve **3** is open, directional valve **4** is in *position b* while **10** is closed. Both pumps **1** and **2** delivery oil in *line R*, feeding pressing cylinders with a flow rate given by (per cylinder):

$$V_1 = \frac{S_1 \dot{h}}{\eta_{cv}} \tag{7}$$

where η_{cv} is the volumetric efficiency of the cylinder, S_1 is the surface related to D_1 and $\dot{h} = \dot{q}_{work}$ (ram speed on phase 3, pressing operation). On discharge line, valves **7** and **8** are fully opened. Values for pressure in each circuit part can be determined taking into account pressure drops distributed along pipes or concentrated in valves. In order to evaluate distributed pressure drops in pipes, Colebrook-White [24] correlation has been used, which relates friction factor to pipe diameter, pipe roughness and Reynolds number. Junctions have been treated with the method of equivalent length pipes. Each type of valve has a different behavior, but essentially it can be assumed that, given a valve spool position, concentrated pressure drops are functions of flow rate. These functions are given by hydraulic manufacturers, and they have been implemented in the model.

Pressure in cylinder chamber 2 (p_2) can be determined

Generally, from here on, variables with subscript 1,2 refers to main cylinders chamber 1,2

starting from tank and adding pressure drops of discharge line. The difference of pressure between cylinder chambers $(p_1 - p_2)$ can be determined by the equilibrium equation of the cylinder rod, namely

$$Q_i + m(\ddot{h} - g) = \eta_{cm}[(p_1 - p_2)S_1 + p_2 S_2] \tag{8}$$

In this phase, pumps can be assumed to act symmetrically, with each of them feeding a single cylinder. Assuming that pump suction is at atmospheric pressure, pumps head Δp_p can easily be determined adding remaining pressure drops given by directional valve **4** and cartridge valve **3**. Finally, mechanical power to provide at pump shafts during pressing phase can be calculated (per pump):

$$P_{wh} = \frac{\Delta p_p V_1}{\eta_{pv}\eta_{pm}} \tag{9}$$

where η_{pv} and η_{pm} are volumetric and mechanical pump efficiencies, respectively.

Since valve **10** is closed in pressing phase (*position 0*), valve **11** regulates die cushion counter-force (pressure control) while cylinder **12** is driven by top ram. During ram positioning (i.e. falling phase), Eqn. 8 is still valid. Setting the maximum value of acceleration to $\ddot{h} = 1\,\frac{\mathrm{m}}{\mathrm{s}^2}$ to match standard cycle times (maximum value for falling velocity is set to $\dot{h} = 0.15\frac{m}{s}$), the term $m(\ddot{h} - g)$ is always negative. Thus, $p_2 > p_1$ as the cylinder brakes the ram mass. Pressure p_2 is controlled by **7**, while proportional valve **8** controls flow rate, thus speed. Pressure p_1 may be considered to be atmospheric, as the connection with a pre-filled tank is operated by valve **13**. Therefore, pumps head Δp_p is equal to circuit losses in pipes and valves **3** and **4**.

After operation, the system is restored to initial position (lifting phase). Both pressing ram and die cushion have to be lifted up, the first for all the stroke (600 mm), the latter for half the stroke (300 mm). To do this, valve **3** is closed, pump **1** delivers oil in *line R*, while pump **2** delivers oil in *line L*, working independently. Pump **1** feed the cylinder in chamber 2 through check valve **9** and valve **7**, with a flow rate:

$$V_2 = \frac{\eta_{pv} n_p c_{max}}{60} \tag{10}$$

where c_{max} is the maximum value of displacement, in order to complete the cycle as soon as possible; n_p is the pump shaft rotational speed. Pump head Δp_p, again, can be calculated with Eqn. 8 and taking into account circuit drops. *Line L* works differently. Pump **2** works at maximum flow rate (as in Eqn. 10), while directional valve **10** is in *position b*. Die cushion cylinder chambers are connected and they share the same pressure; thus, lifting force is granted by the difference of piston and rod areas. While valve **11** is maintained closed, the oil expelled from the output chamber is reintegrated in *line L* itself by valve **10**, improving considerably total flow rate, thus lifting speed.

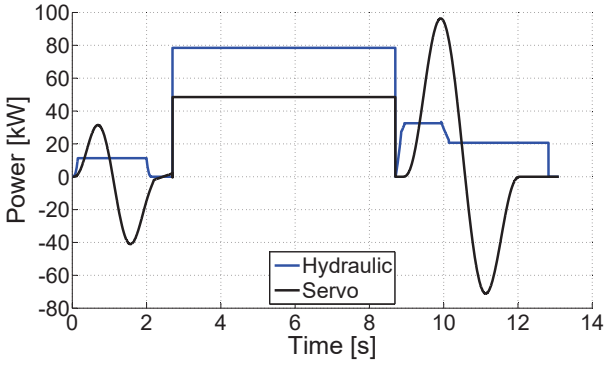

Fig. 12. Power comparison between the servo press and its hydraulic equivalent

4.3 Mechanical Power comparison

In Fig. 12, the mechanical power required during a full cycle of the hydraulic press is shown. Mechanical energy exchanged by servo architecture press is shown as well (cf. Fig. 10). The three phases (falling, working, lifting) discussed previously can be easily recognized. During lifting, a drop on power requirement of the hydraulic press can be noticed around $t = 10$ s; in fact, pump **2** completes its task faster because flow rate is delivered entirely to cylinder **12**, unlike pump **1** flow rate, which is shared by cylinders; furthermore, die cushion stroke is half the value of total ram stroke, resulting in a faster repositioning.

Several considerations on mechanical energy can be made comparing the two technologies. Mechanical energy needed to complete a press cycle with the hydraulic architecture is $E_{hyd} = 590.34$ kJ. Assuming to recover all the energy given back by the servo press prototype, the energy needed for a cycle is $E_{el} = 310.9$ kJ, saving up to 47.8% of total energy. Considering only positioning phases, where only dynamics loads are present, the difference is even more conspicuous: 119.6 kJ for hydraulic against 20.6 kJ for servo (saving 83.3%); in fact, virtually, all the energy given to accelerate the system in a conservative force field can be almost entirely recovered. Even neglecting the contribution of the recovery system (i.e. assuming to dissipate the energy returned by the servo press during the ram deceleration), the overall efficiency still favors servo technology. Indeed, the corresponding value for power would be $E_{el_{norec}} = 537.11$ kJ, which achieves a saving of 9%. This difference can be accounted for energy conversion losses: these are higher when converting from electric energy to hydraulic, and from this to mechanical.

5 Conclusions

A family of non-overconstrained architectures has been proposed for multi-axis servo presses. It has been shown that an n-dof parallel mechanism may be employed to realize such an arrangement, with $2 \leq n \leq 6$. The proposed architecture is completely modular, so that servo actuated axes and corresponding legs can be designed and sized irrespective of the global press size. In this way, larger pressing forces can be achieved using multi-axial layouts. Furthermore, a non-overconstrained architecture prevents all issues

related to redundant actuation (e.g. motors working in conflict, additional internal stresses on press frame, variation of ball-screw preload), which may limit press performances or even lead to press failure.

A detailed study of a biaxial servo press has been presented and a biaxial prototype has been built. It has been shown that such a non-overconstrained multi-axis press can be constructed from commercially available components, achieving high energy efficiency and high press force with relatively simple construction. It has also been proven that energy recovery may be a positive aspect of the servo-actuated system, improving system efficiency compared to equivalent hydraulic arrangements.

6 Acknowledgments

The authors gratefully acknowledge the financial support of the Italian Ministry of Economic Development through the Industry 2015 grant No. 00065MI01. They also wish to express their gratitude to the industrial partners of the *DEFCOM* project, in particular Gigant Italia, which built the prototype and provided the CAD drawings presented in Fig.4.

References

[1] Kirecci, A., and Dulger, L. C., 2000. "A study on a hybrid actuator". *Mechanism and Machine Theory,* **35**(8), pp. 1141–1149.

[2] Li, H., and Zhang, Y., 2010. "Seven-bar mechanical press with hybrid-driven mechanism for deep drawing; Part 1: kinematics analysis and optimum design". *Journal of Mechanical Science and Technology,* **24**(11), pp. 2153–2160.

[3] Li, H., Fu, L., and Zhang, Y., 2010. "Optimum design of a hybrid-driven mechanical press based on inverse kinematics". *Journal of Mechanical Engineering,* **56**(5), pp. 301–306.

[4] Soong, R. C., 2010. "A new design method for single dof mechanical presses with variable speeds and length-adjustable driving links". *Mechanism and Machine Theory,* **45**(3), pp. 496–510.

[5] KOMATSU, 2012. *Komatsu H1FHybrid Ac servo press*. http://www.komatsupress.com/Komatsu/Main/.

[6] Du, R., and Guo, W., 2003. "The design of a new metal forming press with controllable mechanism". *ASME Journal of Mechanical Design,* **125**(3), pp. 582–592.

[7] Guo, W., and Du, R., 2005. "A new type of controllable mechanical press-motion control and experimental validation". *ASME Journal of Manufacturing Science and Engineering,* **127**(4), pp. 731–742.

[8] Osakada, K., Mori, K., Altan, T., and Groche, P., 2011. "Mechanical servo press technology for metal forming". *CIRP Annals - Manufacturing Technology,* **60**(2), pp. 651–672.

[9] Miyoshi, K., 2004. "Current trends in free motion presses". In 3rd JSTP International Seminar on Precision Forging, pp. 69–74. March 15-18, Nagoya, Japan.

[10] Merlet, J., 2006. *Parallel Robots*. Springer, Dordrecht, Netherlands.

[11] Bai, Y., Gao, F., and Guo, W., 2009. "The design of a PKM-type composite actuator for servo mechanical presses". In ASME/IFToMM International Conference on Reconfigurable Mechanisms and Robots, pp. 243–250. 22-24 June 2009, London.

[12] Bai, Y., Gao, F., and Guo, W., 2011. "Design of mechanical presses driven by multi-servomotor". *Journal of Mechanical Science and Technology,* **25**(9), pp. 2323–2334.

[13] Gao, F., and Guo, W., 2009. "Design of a servo mechanical press with redundant actuation". *Chinese Journal of Mechanical Engineering,* **22**(4), pp. 574–580.

[14] Bai, Y., Gao, F., Guo, W., and Yue, Y., 2012. "Kinematic and dynamic analyses of the multi-actuated mechanical press with parallel topology". *Journal of Mechanical Engineering Science,* **226**(10), pp. 2573–2588.

[15] Carricato, M., and Parenti-Castelli, V., 2004. "The topological and geometrical synthesis and classification of translational parallel mechanisms". In 11th World Congress in Mechanism and Machine Science, pp. 1624–1628.

[16] Blanding, D. L., 1999. *Exact Constraint: Machine Design Using Kinematic Principles*. ASME press, New York.

[17] Gosselin, C., and Kong, X., 2007. *Type Synthesis of Parallel Mechanisms*. Springer, Dordrecht, Netherlands.

[18] Carricato, M., and Conconi, M., 2009. "A new assesment of singularities of parallel kinematic chains". *IEEE Transactions on Robotics,* **25**(4), pp. 757–770.

[19] Clavel, R., 1990. "Device for the movement and positioning of an element in space". US Patent 4976582.

[20] TTS, 2012. *DefCom - Industry 2015*. http://web.ttsnetwork.net/DEFCOM/pages/index.jsp.

[21] SIEMENS, 2012. *Main Motors for SINAMICS S120*. http://www.industry.siemens.com/drives/global/en/motor/, May.

[22] ROSSI GROUP, 2011. *G05-Parallel (standard and long) and right angle shaft gear reducers and gearmotors*. http://www.rossi-group.com/index, June.

[23] UMBRA CUSCINETTI, 2011. *Ballscrew for Industrial Applications, Dimensional Tables*. http://www.umbragroup.it/en/home, June.

[24] Colebrook, C. F., and White, C. M., 1939. "Experiments with fluid-friction in roughened pipes". *Proc. Royal Soc. London,* **161**, pp. 367–381.